

# RSC Advances



This is an *Accepted Manuscript*, which has been through the Royal Society of Chemistry peer review process and has been accepted for publication.

*Accepted Manuscripts* are published online shortly after acceptance, before technical editing, formatting and proof reading. Using this free service, authors can make their results available to the community, in citable form, before we publish the edited article. This *Accepted Manuscript* will be replaced by the edited, formatted and paginated article as soon as this is available.

You can find more information about *Accepted Manuscripts* in the [Information for Authors](#).

Please note that technical editing may introduce minor changes to the text and/or graphics, which may alter content. The journal's standard [Terms & Conditions](#) and the [Ethical guidelines](#) still apply. In no event shall the Royal Society of Chemistry be held responsible for any errors or omissions in this *Accepted Manuscript* or any consequences arising from the use of any information it contains.

# A new hard phase and physical properties of Tc<sub>2</sub>C predicted from first principles

Gangtai Zhang,<sup>a</sup> Yaru Zhao,<sup>a</sup> Tingting Bai,<sup>b</sup> Qun Wei,<sup>c</sup> and Yuquan Yuan<sup>d,\*</sup>

**Abstract:** Using the first principles particle swarm optimization algorithm for crystal structural prediction, we have predicted a hexagonal  $P6_3/mmc$  structure of Tc<sub>2</sub>C. The new phase is mechanically and dynamically stable, as verified by its elastic constants and phonon dispersion. The formation enthalpy-pressure curves show that the predicted  $P6_3/mmc$ -Tc<sub>2</sub>C is more energetically favorable than the previously proposed Mo<sub>2</sub>C-, anti-MoS<sub>2</sub>-, Re<sub>2</sub>P-, and Fe<sub>2</sub>N-type structures in the considered pressure range. The calculated mechanical properties exhibit that it is an ultra-incompressible and hard material. Meanwhile, the directional dependences of the Young's modulus, bulk modulus, and shear modulus for Tc<sub>2</sub>C are systematically investigated. The analyses of density of states and electronic localization function reveal the presence of strong covalent bonding between Tc and C atoms, which is of crucial importance in forming a hard material.

## 1. Introduction

Designing and searching for ultra-incompressible and superhard materials are of great scientific interests due to their various industrial applications, such as cutting and polishing tools, abrasives, oil exploitations, and coatings. Previously, it was generally accepted that the superhard materials are strong covalent bonded compounds formed by light atoms B, C, N, and O, such as diamond,<sup>1</sup> *c*-BN,<sup>2</sup> B<sub>6</sub>O,<sup>3</sup> etc. These materials are easily to form strong three-dimension covalent bonding networks. Though diamond is the hardest known material with a measured hardness of 60~120GPa, it is unstable in the presence of oxygen at a moderate temperature and reacts easily with iron-based materials. The second-hardest material is cubic boron nitride (*c*-BN), but it can be synthesized only under high temperature and high temperature conditions, which needs great cost of synthesis. Thus, intense effort has

---

<sup>a</sup>College of Physics and Optoelectronics Technology, Baoji University of Arts and Sciences, Baoji 721016, PR china

<sup>b</sup>College of Mathematics and Information Science, Baoji University of Arts and Sciences, Baoji 721013, PR China

<sup>c</sup>School of Physics and Optoelectronic Engineering, Xidian University, Xi'an 710071, PR China

<sup>d</sup>School of Science, Sichuan University of Science and Engineering, Zigong 643000, PR China

Email: [yuquan\\_yuan1975@suse.edu.cn](mailto:yuquan_yuan1975@suse.edu.cn) (Y.Q. Yuan)

been devoted for hunting the new hard and ultra-incompressible materials. Recently, it has been reported that the incorporation of light atoms (B, C, N and O) into heavy transition metals (TMs) with high valence electron densities provides a good candidate for designing new hard materials. The compounds formed by transition metal and light atoms usually possess high valence electron density and directional covalent bonds, and these covalent bonds are strong enough to inhibit creation and movement of dislocations, which significantly improve their mechanical properties and create high hardness. Following this design criterion, recent design of the new intrinsically potential superhard materials has focused on light element TM compounds, e.g.  $\text{ReB}_2$ ,<sup>4</sup>  $\text{WC}$ ,<sup>5</sup>  $\text{IrN}_2$ ,<sup>6</sup>  $\text{RuO}_2$ <sup>7</sup> and so on, the obtained results show that these materials usually possess the large bulk and shear moduli. Thereby, these pioneering studies open up a new route for pursuing new superhard materials

Carbides, especially TM carbides, are widely used for industrial application because of their high melting temperature, extreme hardness, and chemical stability, which makes them useful in cutting tools, dental drills, rock drills in mining, and abrasives. Experimentally, some monocarbides, such as  $\text{TiC}$ ,<sup>8</sup>  $\text{ZrC}$ ,<sup>9</sup>  $\text{PtC}$ ,<sup>10</sup> and  $\text{WC}$ <sup>5</sup> have been synthesized, the obtained results show that they all hold very bulk modulus. A high bulk modulus is a good indicator of a superhard material, thus TM carbides are potential candidates for superhard materials.  $\text{Re}_2\text{C}$  belongs to the family of TM carbides, and some experimental and theoretical studies of  $\text{Re}_2\text{C}$  have been investigated.<sup>11-15</sup> Meanwhile, these theoretical calculations and experimental data reveal that  $\text{Re}_2\text{C}$  is ultra-incompressible and has a high bulk module of about 400GPa.

Technetium (Tc) lies directly above Re in the periodic table and has the same valence electron number, so it is worth studying the mechanical properties of its carbides. Experimentally,  $\text{TcC}$  has been first synthesized in 1962 and was presumed to be hexagonal and faced-centred cubic structures.<sup>16</sup> Later, Giorgi and Szklarz interpreted the cubic compound on the authority of a body-centred cubic phase.<sup>17</sup> Recently, an experimental synthesis has verified the existence of  $\text{TcC}$ ,<sup>18</sup> which also provides a useful information for understanding the crystal structure of  $\text{TcC}$ . Theoretically, the crystal structures and the related physical properties of  $\text{TcC}$  have been considerably investigated.<sup>19-25</sup> These calculated results indicated that  $\text{TcC}$  with considered structures is an ultra-incompressible and hard material. However, the research works of the compounds with lower carbon contents are seldom reported so far.

In this paper, we have extensively investigated the ground state structure of  $\text{Tc}_2\text{C}$  by using the first principles particle swarm optimization algorithm (PSO) on crystal structural prediction.<sup>26</sup> This method has been successfully applied to various systems,<sup>27–29</sup> unbiased by any known information. A novel hexagonal  $P6_3/mmc$  structure is uncovered for  $\text{Tc}_2\text{C}$ , which is more energetically favorable than the earlier proposed  $\text{Mo}_2\text{C}$ -, anti- $\text{MoS}_2$ -,  $\text{Re}_2\text{P}$ -, and  $\text{Fe}_2\text{N}$ -type structures in the pressure range of 0–120 GPa. First principles calculations are then performed to study the total energy, lattice parameters, phase stability, elastic properties, elastic anisotropy, and density of states for this novel hexagonal phase.

## 2. Computational methods

The PSO technique for crystal structural prediction has been implemented in the crystal structure analysis by the particle swarm optimization (CALYPSO) code<sup>30</sup> at 0 GPa with 1-4 formula units (f.u.) each simulation cell. The underlying *ab initio* calculations are performed using density functional theory as implemented in the Vienna *ab initio* simulation package (VASP).<sup>31</sup> The generalized gradient approximation (GGA) is used for the exchange and correlation potentials. The all-electron projector augmented wave (PAW) method<sup>32</sup> is employed with  $2s^22p^2$  and  $4p^64d^55s^2$  treated as the valence electrons for C and Tc, respectively. Geometry optimization is performed by using the conjugate gradient algorithm method with a plane-wave cutoff energy of 520 eV. The calculations are conducted with  $14 \times 14 \times 4$ ,  $14 \times 14 \times 4$ ,  $8 \times 6 \times 7$ ,  $14 \times 14 \times 4$ ,  $7 \times 12 \times 4$ , and  $14 \times 14 \times 4$  for the predicted  $P6_3/mmc$ - $\text{Tc}_2\text{C}$  structure and our considered anti- $\text{ReB}_2$ -type (space group  $P6_3/mmc$ ),  $\text{Mo}_2\text{C}$ -type (space group  $Pbcn$ ), anti- $\text{MoS}_2$ -type (space group  $P6_3/mmc$ ),  $\text{Re}_2\text{P}$ - type (space group  $Pnma$ ), and  $\text{Fe}_2\text{N}$ -type (space group  $P-3m1$ ) structures, respectively. For hexagonal structures,  $\Gamma$  centered  $k$  mesh is adopted, and for other structures, Monkhorst-Pack  $k$  meshes<sup>33</sup> are used to ensure that all the total energy calculations are well converged to better than 1 meV/atom. The phonon calculation is carried out by using a supercell approach as implemented in the PHONOPY code.<sup>34</sup> Single crystal elastic constants are calculated by a strain-energy approach, i.e., applying a small strain to the equilibrium lattice and fitting the dependence of the resulting change in energy on the strain. The bulk modulus, shear modulus, Young's modulus, and Poisson's ratio are derived from the Voigt–Reuss–Hill approximation.<sup>35</sup>

### 3. Results and discussion

Using the PSO technique, we perform variable-cell structure prediction simulation for  $\text{Tc}_2\text{C}$  containing 1-4 f.u. in the simulation cell at 0 GPa, a hexagonal  $P6_3/mmc$  structure is found, as shown in Fig. 1. The  $P6_3/mmc$  structure contains two  $\text{Tc}_2\text{C}$  f.u. in a unit cell. At ambient pressure, the equilibrium lattice parameters are  $a=b=2.838 \text{ \AA}$  and  $c=9.774 \text{ \AA}$ , in which the Tc and C atoms occupy Wyckoff  $4f(1/3, 2/3, 0.89092)$  and  $2c(1/3, 2/3, 1/4)$  sites, respectively. From Fig. 1(a), each C atom is coordinated by 6 neighboring Tc atoms, forming edge-shared  $\text{Tc}_6\text{C}$  trigonal prisms with Tc-C bond distance of  $2.141 \text{ \AA}$ , which is shorter than the Re-C ( $2.16 \text{ \AA}$ ) and Os-C distance ( $2.32 \text{ \AA}$ ) in hard materials  $\text{Re}_2\text{C}^{11}$  and  $\text{Os}_2\text{C}^{36}$  respectively. To check the structural stability of the new phase of  $\text{Tc}_2\text{C}$ , the phonon dispersion curves are calculated at 0 GPa and 120 GPa, respectively, and the results are given in Fig. 2. Clearly, the  $P6_3/mmc$  structure is dynamically stable at ambient pressure and high pressure because of the inexistence of the imaginary phonon frequency in the whole Brillouin zone. It is well known that the thermodynamic stability of a compound can be described by the knowledge of its ground-state energy. Therefore, we calculate the total energy per f.u. as a function of the volume for the predicted  $P6_3/mmc$  structure. For comparison, the previously known five structures of anti- $\text{ReB}_2$ ,  $\text{Mo}_2\text{C}$ , anti- $\text{MoS}_2$ ,  $\text{Re}_2\text{P}$ , and  $\text{Fe}_2\text{N}$  are also considered for  $\text{Tc}_2\text{C}$ . The calculated results are shown in Fig. 3. As seen from this figure, the predicted  $P6_3/mmc$  structure for  $\text{Tc}_2\text{C}$  has the lower energy minimum than the  $\text{Mo}_2\text{C}$ -, anti- $\text{MoS}_2$ -,  $\text{Re}_2\text{P}$ -, and  $\text{Fe}_2\text{N}$ -type structures but the same energy-volume curve as the anti- $\text{ReB}_2$ -type structure. On the one hand, this indicates that the predicted  $P6_3/mmc$  structure is the ground-state phase at 0 GPa. On the other hand, this confirms that the  $P6_3/mmc$ - $\text{Tc}_2\text{C}$  has the same structure with anti- $\text{ReB}_2$ .

To explore the thermodynamic stability for further experimental synthesis, the formation enthalpy of the  $\text{Tc}_2\text{C}$  with respect to the separate phases is examined by the reaction route  $\Delta H = H_{\text{Tc}_2\text{C}} - 2H_{\text{Tc}} - H_{\text{C}}$ , here  $\Delta H$  is the formation enthalpy, the hexagonal Tc (space group:  $P6_3/mmc$ ) and the graphite C are chosen as the reference phases. The calculated formation enthalpy under pressure is shown in Fig. 4. As shown in this figure, the stabilities of  $\text{Tc}_2\text{C}$  with different structures are gradually enhanced with increasing the pressure, therefore, the pressure is helpful to their stabilities. At ambient condition, the negative values of the

formation enthalpies for the predicted  $P6_3/mmc$ -Tc<sub>2</sub>C and anti-ReB<sub>2</sub>-type structures indicate that they are thermodynamically stable, whereas the positive formation enthalpies for other structures show that they are not thermodynamically stable. Moreover, it can be seen that the enthalpy-pressure curves of the  $P6_3/mmc$ - and anti-ReB<sub>2</sub>-type structures merge together in our considered pressure range, which further proves that they belong to the same structure. The present calculated results suggest that the predicted  $P6_3/mmc$ -Tc<sub>2</sub>C can be synthesized at ambient condition, thus further experimental synthesis is highly desirable.

As is well known, the mechanical stability is a necessary condition for the stabilization of a crystal to exist, and the mechanical properties, such as elastic constants and elastic moduli, are important for potential technological and industrial applications. Thus we perform further the studies on the mechanical properties of the  $P6_3/mmc$ -Tc<sub>2</sub>C phase. By using a strain-energy method, we obtain the zero-pressure elastic constants ( $C_{ij}$ ) of the  $P6_3/mmc$ -Tc<sub>2</sub>C and  $P-6m2$ -TcC, respectively. The calculated elastic constants  $C_{ij}$  are listed in Table 1, along with the theoretical values and available experimental data of other TM carbides (WC,<sup>5</sup> PtC,<sup>10</sup> Re<sub>2</sub>C,<sup>11,12,14,15</sup> Ru<sub>2</sub>C,<sup>37,38</sup> and Os<sub>2</sub>C<sup>36,39</sup>) for comparison. For a stable hexagonal crystal,  $C_{ij}$  should satisfy the following criteria:<sup>40</sup>  $C_{33}>0$ ,  $C_{44}>0$ ,  $C_{12}>0$ ,  $C_{11}>|C_{12}|$ ,  $(C_{11}+2C_{12})C_{33}>2C_{13}^2$ . As shown in Table 1, the elastic constants of the predicted  $P6_3/mmc$ -Tc<sub>2</sub>C satisfy completely the elastic stability criteria for a hexagonal crystal, thus it is mechanically stable at ambient condition. The large values of  $C_{11}$  and  $C_{33}$  for the compound suggest that it is extremely difficult to be compressed along  $a$ -axis (or  $b$ -axis) and  $c$ -axis, respectively. Moreover, the  $C_{33}$  value of the  $P6_3/mmc$  phase (781 GPa) is close to those for WC,<sup>5</sup> TcC,<sup>19-21</sup> and Re<sub>2</sub>C<sup>11</sup> but much larger than Ru<sub>2</sub>C<sup>38</sup> and Os<sub>2</sub>C,<sup>39</sup> suggesting its high linear incompressibility along the  $c$ -axis. Based on the obtained elastic constants  $C_{ij}$ , the polycrystalline bulk modulus  $B$  and shear modulus  $G$  are thus determined by the Voigt–Reuss–Hill approximation. The Young's modulus  $E$  and Poisson's ratio  $\nu$  can be derived by the following equations  $E=9BG/(3B+G)$  and  $\nu=(3B-2G)/(6B+2G)$ . The calculated bulk modulus, shear modulus, Young's modulus, and Poisson's ratio of the  $P6_3/mmc$  phase together with the reference materials mentioned above are listed in Table 1. As shown in Table 1, the bulk modulus of the  $P6_3/mmc$  phase is 343 GPa, which is comparable to the experimental data of WC (439 GPa),<sup>5</sup> PtC (301(±15)),<sup>10</sup> and Re<sub>2</sub>C (405(30) and 386(10))<sup>14,15</sup> but much more higher than that of Ru<sub>2</sub>C (178(4) GPa),<sup>37</sup> indicating

its ultra-incompressible structure nature. Moreover, the calculated bulk modulus ( $B=343$  GPa) for the  $P6_3/mmc$ - $Tc_2C$  agrees well with that directly obtained from the fitting results ( $B_0=344$  GPa) of the third-order Birch-Murnaghan equation of states, further verifying the reliability of the present elastic calculations. In order to further compare the incompressibility of the  $P6_3/mmc$ - $Tc_2C$ , WC, PtC,  $Re_2C$ , and  $Ru_2C$  under pressure, the volume compressions as a function of the pressure are presented in Fig. 5. It can be seen that the volume incompressibility of the  $P6_3/mmc$ - $Tc_2C$  is comparable to those of WC and  $Re_2C$  but exceeds those of PtC and  $Ru_2C$ . Compared with the bulk modulus, the shear modulus of a material quantifies its resistance to the shear deformation and acts as a better indicator of the potential hardness. Obviously, the predicted  $P6_3/mmc$  phase has a large shear modulus of 216 GPa, thus it is expected to withstand the shear strain to a large extent. In addition, Young's modulus can also provide a good measure of the stiffness of materials except the bulk modulus and shear modulus. The larger Young's modulus the material has, the harder it is to deform. The calculated Young's modulus of the  $P6_3/mmc$ - $Tc_2C$  is 536 GPa, indicating that it is a hard material. Poisson's ratio  $\nu$  is a crucial parameter to describe the degree of directionality of the covalent bonding. Generally speaking, the typical  $\nu$  value is 0.1 for covalent materials and 0.33 for metal materials, respectively. From Table 1, it can be seen that the  $\nu$  value of the  $P6_3/mmc$ - $Tc_2C$  phase is below 0.33 and at the same time the  $P6_3/mmc$ - $Tc_2C$  has the smallest Poisson's ratio 0.239 in contrast to other considered TM carbides, such as  $Ru_2C$ ,<sup>38</sup>  $Os_2C$ ,<sup>39</sup> and  $TcC$ .<sup>19-21</sup> Consequently, the  $P6_3/mmc$ - $Tc_2C$  has a strong degree of covalent bonding. Furthermore, the  $B/G$  ratio is commonly used to predict the brittle or ductile behavior of materials. According to the Pugh criterion,<sup>41</sup> if  $B/G > 1.75$ , the material behaves in a ductile way, otherwise, the material behaves in a brittle manner. For the case of the  $P6_3/mmc$ - $Tc_2C$ , our predicted value of  $B/G$  is 1.59, suggesting that it has a little brittle nature. Using the empirical formula for the hardness prediction proposed by Chen *et al.*,<sup>42</sup> the estimated Vickers hardness for the  $P6_3/mmc$ - $Tc_2C$  is 24.11 GPa, which is comparable to the known hard materials of  $SiO_2$  (30.6 GPa)<sup>43</sup> and  $B_4C$  (32.8 GPa).<sup>44</sup> All of these excellent mechanical properties strongly support that the  $P6_3/mmc$ - $Tc_2C$  is an ultra-incompressible and hard material.

For engineering applications that make use of single crystals, it is necessary to know the values of the Young's modulus, bulk modulus, and shear modulus as a function of crystal

orientation. For the hexagonal  $P6_3/mmc$ - $Tc_2C$ , the Young's modulus and bulk modulus are expressed by:

$$E^{-1} = s_{11}(\alpha^2 + \beta^2)^2 + s_{33}\gamma^4 + (2s_{13} + s_{44})(\beta^2\gamma^2 + \alpha^2\gamma^2), \quad (1)$$

$$B^{-1} = (s_{11} + s_{12} + s_{13}) - (s_{11} + s_{12} - s_{13} - s_{33})\gamma^2, \quad (2)$$

where  $\alpha$ ,  $\beta$ , and  $\gamma$  are the direction cosines of  $[uvw]$  direction and  $s_{ij}$  are the elastic compliance constants which are obtained by Nye.<sup>45</sup> The shear modulus on the  $(hkl)$  shear plane with the shear stress applied along the  $[uvw]$  direction is written as

$$G^{-1} = 4s_{11}(\alpha_1^2\alpha_2^2 + \beta_1^2\beta_2^2) + 4s_{33}\gamma_1^2\gamma_2^2 + 8s_{12}\alpha_1\alpha_2\beta_1\beta_2 + 8s_{13}(\alpha_1\alpha_2 + \beta_1\beta_2)\gamma_1\gamma_2 + s_{44}[(\beta_1\gamma_2 + \beta_2\gamma_1)^2 + (\alpha_1\gamma_2 + \alpha_2\gamma_1)^2] + s_{66}(\alpha_1\beta_2 + \alpha_2\beta_1)^2, \quad (3)$$

where  $\alpha_1$ ,  $\beta_1$ ,  $\gamma_1$ ,  $\alpha_2$ ,  $\beta_2$ ,  $\gamma_2$  are the direction cosines of the  $[uvw]$  and  $[hkl]$  directions in the coordinate systems, and the  $[hkl]$  direction shows the vector normal to the  $(hkl)$  shear plane.

Fig. 6(a) and (c) are the three-dimensional surface representations which show the variation of the Young's modulus and bulk modulus, respectively. For an isotropic crystal, one would see a spherical shape, while a deviation from a spherical shape can directly reflect the degree of the elastic anisotropy in the crystal. From these two figures, one can see that the Young's modulus exhibits a high degree of the elastic anisotropy due to a large deviation from a spherical shape, whereas the bulk modulus is nearly isotropic because of a small deviation from a spherical shape. The projections of the Young's modulus and bulk modulus on the  $ab$  and  $bc$  planes are also plotted in Fig. 6(b) and (d) for comparison. As can be seen, in-plane anisotropy in the  $ab$  plane is not existent, whereas in-plane anisotropy in the  $bc$  plane is directly revealed. A deeper insight of the change of the Young's modulus along different directions can be obtained by investigating the directional dependences of the Young's modulus along tensile axis in the  $(0001)$ ,  $(10\bar{1}0)$ ,  $(\bar{1}2\bar{1}2)$ , and  $(\bar{1}012)$  planes, respectively, and the obtained results are given in Fig. 7(a). For the  $(0001)$  plane, since the direction cosines are  $\alpha = \cos\theta$ ,  $\beta = \sin\theta$ , and  $\gamma = 0$  ( $\theta$  is the angle between tensile stress and  $[0001]$ ), one obtains  $E^{-1} = s_{11}$  from Eq. (1). This implies that the Young's modulus on the basal plane is independent of the tensile stress direction for the  $P6_3/mmc$ - $Tc_2C$ , which is the reason of the elastic isotropy in the basal plane for hexagonal crystal. For the directional dependences of the Young's modulus from  $[0001]$  to  $[\bar{1}2\bar{1}0]$  in the  $(10\bar{1}0)$  plane, the

$P6_3/mmc$ - $Tc_2C$  possesses a maximum of  $E_{[0001]} = 708.2$  GPa and a minimum of  $E_{[\bar{1}2\bar{1}0]} = 527.8$  GPa. For the  $(\bar{1}2\bar{1}2)$  plane, the Young's modulus along the  $[10\bar{1}0]$  direction has the minimal value ( $E_{\min} = 527.8$  GPa) and the Young's modulus along the  $[\bar{1}2\bar{1}1]$  direction has the maximal one ( $E_{\max} = 653.6$  GPa). For the change of the Young's modulus in the  $(\bar{1}012)$  plane for the quadrant of directions between  $[\bar{1}2\bar{1}0]$  and  $[10\bar{1}1]$ , the  $P6_3/mmc$ - $Tc_2C$  exhibits a maximum of  $E_{[10\bar{1}1]} = 591.7$  GPa and a minimum of  $E_{[\bar{1}2\bar{1}0]} = 527.8$  GPa. Consequently, the order of the Young's modulus as a function of the principal crystal tensile  $[uvw]$  for the  $P6_3/mmc$ - $Tc_2C$  is:  $E_{[0001]} > E_{[\bar{1}2\bar{1}1]} > E_{[10\bar{1}1]} > E_{[10\bar{1}0]}$ . To understand the plastic deformation for the predicted  $P6_3/mmc$ - $Tc_2C$  phase, we investigate the dependence of the shear modulus on the stress direction, and the corresponding result is presented in Fig. 7(b). For the  $(0001)$  shear plane with the shear stress direction varied from  $[10\bar{1}0]$  to  $[\bar{1}2\bar{1}0]$ , since the direction cosines are  $\alpha_1 = \beta_1 = 0, \gamma_1 = 0, \alpha_2 = \cos\theta, \beta_2 = \sin\theta$ , and  $\gamma_2 = 0$  ( $\theta$  is the angle between the shear direction and  $[10\bar{1}0]$ ), one can obtain  $G^{-1} = s_{44}$  from Eq. (3). This implies that the shear modulus is isotropic in the basal plane, as shown by the green curve in Fig. 7(b). For the shear plane  $(10\bar{1}0)$  with the shear stress direction changed from  $[0001]$  to  $[\bar{1}2\bar{1}0]$ ,  $\alpha_1 = 1, \beta_1 = \gamma_1 = 0, \alpha_2 = 0, \beta_2 = \sin\theta$ , and  $\gamma_2 = \cos\theta$  ( $\theta$  is the angle between the shear direction and  $[0001]$ ), so the shear module can be reduced to  $G^{-1} = s_{66} + (s_{44} - s_{66})\cos^2\theta$ . Since  $s_{44} > s_{66}$  in our calculations, the shear module on the  $(10\bar{1}0)$  plane is the highest when  $\theta = 90^\circ$  and the lowest when  $\theta = 0$ , corresponding to  $G_{\max} = 205.5$  GPa for the  $[\bar{1}2\bar{1}0]$  direction and  $G_{\min} = 199$  GPa for the  $[0001]$  direction. For the shear plane  $(\bar{1}2\bar{1}2)$  with the shear stress direction rotated from  $[10\bar{1}0]$  to  $[\bar{1}2\bar{1}1]$ , the maximum of the shear modulus is 212.6 GPa for the  $[\bar{1}2\bar{1}1]$  direction and the minimum of the shear modulus is 204.9 GPa for the  $[10\bar{1}0]$  direction. When the pyramidal plane  $(\bar{1}012)$  is the shear plane and the shear stress direction is

changed from  $[\bar{1}2\bar{1}0]$  to  $[10\bar{1}1]$ , the shear modulus is the largest along the  $[10\bar{1}1]$  direction ( $G_{\max} = 232.4$  GPa) and the shear modulus is the smallest along the  $[\bar{1}2\bar{1}0]$  direction ( $G_{\min} = 204.2$  GPa). Through the above analysis, we draw conclusions: (1) the Young's modulus and shear modulus are constant on the basal plane and orientation-dependent on both the pyramidal and prismatic planes; (2) the bulk modulus is almost isotropic.

The elastic anisotropy of crystals can exert great effects on the properties of the physical mechanism, such as anisotropic plastic deformation, crack behavior, and elastic instability. Therefore, it is important and necessary to investigate the elastic anisotropy to improve their mechanical durability. The compression and the shear anisotropic factors provide the measures of the degrees of anisotropy in atomic bonding in different crystallographic planes. For hexagonal crystal, the anisotropies in compressibility and shear are defined as:

$$A_{\text{comp}} = \frac{s_{33} + 2s_{13}}{s_{11} + s_{12} + s_{13}}, \quad (4)$$

$$A_{\text{shear}} = \frac{2c_{44}}{c_{11} - s_{12}}. \quad (5)$$

For an isotropic crystal, the factors  $A_{\text{comp}}$  and  $A_{\text{shear}}$  must be one, while any departure from one is a measure of the degree of elastic anisotropy possessed by the crystal. According to the above definitions, the values of  $A_{\text{comp}}$  and  $A_{\text{shear}}$  are calculated to be 0.77 and 0.968, respectively. This indicates that the  $P6_3/mmc\text{-Tc}_2\text{C}$  phase has a certain degree elastic anisotropy.

Debye temperature is related to many physical properties of materials, such as specific heat, elastic constants, and melting temperature.<sup>46</sup> It is used to differentiate between high and low temperature regions for a solid. When the temperature  $T > \Theta_D$ , all modes are expected to have the energy of  $k_B T$ ; when  $T < \Theta_D$ , the high-frequency modes are expected to be frozen, namely the vibrational excitations origin only from the acoustic vibrations. The Debye temperature  $\Theta_D$  for the studied  $P6_3/mmc\text{-Tc}_2\text{C}$  is estimated from the average sound velocity ( $v_m$ ) by the following equation:

$$\Theta_D = \frac{h}{k} \left[ \frac{3n}{4\pi} \left( \frac{\rho N_A}{M} \right) \right]^{\frac{1}{3}} v_m, \quad (6)$$

where  $h$  is Planck's constant,  $k$  is Boltzmann's constant,  $N_A$  is Avogadro's number,  $n$  is the number of atoms per formula unit,  $M$  is the molecular mass per f.u., and  $\rho$  is the density. The average sound velocity  $v_m$  is given by:

$$v_m = \left[ \frac{1}{3} \left( \frac{2}{v_t^3} + \frac{1}{v_l^3} \right) \right]^{-\frac{1}{3}}, \quad (7)$$

where  $v_t$  and  $v_l$  are the transverse and longitudinal elastic wave velocities of the polycrystalline material, which can be determined by Navier's equation.<sup>47</sup> The obtained Debye temperatures of the  $P6_3/mmc$ -Tc<sub>2</sub>C under pressure are presented in Fig. 8. At zero pressure and zero temperature, the Debye temperature for the predicted  $P6_3/mmc$ -Tc<sub>2</sub>C phase is 675 K. Generally, the higher Debye temperature the materials possess, the larger microhardness they have. From Fig. 8, one can see clearly that the Debye temperature increases with the increase of the pressure. This means that the pressure is better for the enhancement of the hardness for the  $P6_3/mmc$ -Tc<sub>2</sub>C.

The electronic structure is the key to understand the mechanical properties of the  $P6_3/mmc$ -Tc<sub>2</sub>C, the total and partial densities of states (DOS) are calculated and given in Fig. 9, where the vertical dashed line denotes the Fermi level. Distinctly, the  $P6_3/mmc$ -Tc<sub>2</sub>C exhibits a good metallic behavior due to the adequately large total DOS at the Fermi level. This metallicity might make it a better candidate for hard conductors. From partial DOS, it can be clearly seen that the peaks from -13 eV to -10.8 eV are mainly contributed by C-2s and Tc-4d states with small contributions from the 4p and 5s electrons of Tc. The states from -7.3 eV to the Fermi energy (0 eV) mainly originate from the Tc-4d and C-2p orbitals with small contributions of Tc-4p and Tc-5s. In addition, the partial DOS profiles of Tc-4d and C-2p are very similar in the energy region from -7.3 eV to 0 eV, which reflects that Tc-4d orbital has a significant hybridization with C-2p orbital. This fact also shows the existence of a strong covalent bonding between the Tc and C atoms. For the total DOS, the typical feature is the presence of so-called pseudogap, which is regarded as the borderline between the bonding states and antibonding states. Since the Fermi energy is located below the pseudogap for the  $P6_3/mmc$ -Tc<sub>2</sub>C phase, its bonding states are partially occupied and full antibonding states are unoccupied. This property also increases the structural stability of Tc<sub>2</sub>C. Fig. 10 presents the calculated electronic localization function (ELF) of the predicted  $P6_3/mmc$ -Tc<sub>2</sub>C phase on the

(110) plane. From this figure, one can see that the large ELF value between the Tc and C atoms indicates the partially Tc-C covalent bonding interaction in the  $P6_3/mmc$ -Tc<sub>2</sub>C phase. This also explains the reason of the high bulk modulus and large shear modulus of Tc<sub>2</sub>C.

#### 4. Conclusions

In conclusion, a new hexagonal  $P6_3/mmc$  structure is unraveled to be the ground-state structure for Tc<sub>2</sub>C using the PSO algorithm, and it is energetically much superior to the previously known Mo<sub>2</sub>C-, anti-MoS<sub>2</sub>-, Re<sub>2</sub>P-, and Fe<sub>2</sub>N-type structures in the considered pressure range. Based on the calculated phonon dispersion and formation enthalpy curves, we demonstrate that the predicted  $P6_3/mmc$  phase is dynamically stable and synthesizable under the ambient condition. The high bulk modulus, large shear modulus, small Poisson's ratio, and considerable hardness indicate that the  $P6_3/mmc$ -Tc<sub>2</sub>C is an ultra-incompressible and hard material. Moreover, the Young's modulus, bulk modulus, and shear modulus as a function of crystal orientation for Tc<sub>2</sub>C are also investigated systematically. The presence of strong covalent Tc-C bonds, which is of crucial importance in forming a hard material, is confirmed by the detailed analyses of the electronic structure and electronic localization function. We expect that our theoretical results will stimulate further experimental research on this material in the future.

#### Acknowledgement

This work was supported by the Science Foundation of Baoji University of Arts and Sciences of China (Grant Nos. ZK16069 and ZK11135), the Natural Science Foundation of the Education Committee of Shaanxi Province of China (Grant No. 2013JK0637), the Natural Science Basic Research plan in Shaanxi Province of China (Grant No. 2016JM1012), and the Natural Science Foundation of China (Grant No. 11404008).

#### References

- 1 F. Occelli, D.L. Farber and R.L. Toullec, *Nat. Mater.* 2003, **2**, 151.
- 2 Y. Zhang, H. Sun and C.F. Chen, *Phys. Rev. B* 2006, **73**, 144115.
- 3 D.W. He, Y.S. Zhao, L. Daemen, J. Qian, T.D. Shen and T.W. Zerda, *Appl. Phys. Lett.* 2002, **81**, 643.

- 4 H.Y. Chung, M.B. Weinberger, J.B. Levine, A. Kavner, J.M. Yang, S.H. Tolbert and R.B. Kaner, *Science* 2007, **316**, 436.
- 5 M. Lee and R. S. Gilmore, *J. Mater. Sci.* 1982, **17**, 2657.
- 6 J.C. Crowhurst, A.F. Goncharov, B. Sadigh, C.L. Evans, P.G. Morrall, J.L. Ferreira and A.J. Nelson, *Science* 2006, **311**, 1275.
- 7 J.S. Tse, D.D. Klug, K. Uehara, Z.Q. Li, J. Haines and J. M. Léger, *Phys. Rev. B* 2000, **61**, 10029.
- 8 N.A. Dubrovinskaia, L.S. Dubrovinsky, S.K. Saxena, R. Ahuja and B. Johansson, *J. Alloys Compd.* 1999, **289**, 24.
- 9 R. Chang and L.J. Graham, *J. Appl. Phys.* 1966, **37**, 3778.
- 10 S. Ono, T. Kikegawa and Y. Ohishi, *Solid State Commun.* 2005, **133**, 55.
- 11 H. Ozisik, E. Deligoz, K. Colakoglu and G. Surucu, *Phys. Stat. Sol. (RRL)* 2010, **4**, 347.
- 12 Z.S. Zhao, L. Cui, L.M. Wang, B. Xu, Z.Y. Liu, D.L. Yu, J.L. He, X.F. Zhou, H. T. Wang and Y.J. Tian, *Cryst. Growth Des.* 2010, **10**, 5025.
- 13 E.A. Juarez-Arellano, B. Winkler, A. Friedrich, D.J. Wilson, M. Koch-Müller, K. Knorr, S.C. Voge, J.J. Wall, H. Reiche, W. Crichton, M. Ortega-Aviles and M. Avalos-Borja, *Z. Kristallogr.* 2008, **223**, 492.
- 14 E.A. Juarez-Arellano, B. Winkler, A. Friedrich, L. Bayarjargal, V. Milman, J.Y. Yan and S.M. Clark, *J. Alloys Compd.* 2009, **481**, 577.
- 15 N. Yasui, M. Sougawa, M. Hirai, K. Yamamoto, T. Okada, D. Yamazaki, Y. Kojima, H. Ohfujii, S. Kunitsugu and K. Takarabe, *Cogent Physics* 2015, **2**, 1076702.
- 16 W. Trzebiatowski and J.Z. Rudzinski, *Z. Chem.* 1962, **2**, 158.
- 17 A.L. Giorgi and E.G. Szklarz, *J. Less-Common Met.* 1966, **11**, 455.
- 18 V.F. Peretrushin, K.N. Gedgovd, M.S. Grigoriev, A.V. Tarasov, Y.V. Plekhanov, A.G. Maslennikov, G.S. Bulatov, V.P. Tarasov and M. Lecomteb, *J. Nucl. Radiochem. Sci.* 2005, **6**, 211.
- 19 Y. X. Wang, *Phys. Stat. Sol. (RRL)* 2008, **2**, 126.
- 20 Y.C. Liang, C. Li, W.L. Guo and W.Q. Zhang, *Phys. Rev. B* 2009, **79**, 024111.
- 21 Y.C. Zou, J. Zhu, Y.J. Hao, G. Xiang, X.C. Liang and J.R. Wang, *Phys. Status Solidi B* 2014, **251**, 1372.
- 22 X.W. Sun, Y.D. Chu, Z.J. Liu, T. Song, J.H. Tian and X.P. Wen, *Chem. Phys. Lett.* 2014,

- 614, 167.
- 23 T. Song, Q. Ma, J.H. Tian, X.B. Liu, Y.H. Ouyang, C.L. Zhang and W.F. Su, *Mater. Res. Bull.* 2015, **61**, 58.
- 24 M. Kavitha, G.S. Priyanga, R. Rajeswarapalanichamy and K. Iyakutti, *Int. J. Refract. Met. Hard Mater.* 2015, **52**, 219.
- 25 Q.G Wang, K.E. German, A.R. Oganov, H.F. Dong, O.D. Feysa, Y.V. Zubavichus and V.Y. Murzin, *RSC Adv.* 2016, **6**, 16197.
- 26 Y.C. Wang, J. Lv, L. Zhu and Y.M. Ma, *Phys. Rev. B* 2010, **82**, 094116.
- 27 J. Lv, Y.C. Wang, L. Zhu and Y.M. Ma, *Phys. Rev. Lett.* 2011, **106**, 015503.
- 28 L. Zhu, H. Wang, Y.C. Wang, J. Lv, Y.M. Ma, Q.L. Cui, Y.M. Ma and G.T. Zou, *Phys. Rev. Lett.* 2011, **106**, 14550.
- 29 Z.S. Zhao, B. Xu, L.M. Wang, X.F. Zhou, J.L. He, Z.Y. Liu, H.T. Wang and Y.J. Tian, *ACS Nano* 2011, **5**, 7226.
- 30 Y.M. Ma, Y.C. Wang, J. Lv and L. Zhu, <http://nlshm-lab.jlu.edu.cn/~calypso.html>.
- 31 G. Kresse and D. Joubert, *Phys. Rev. B* 1999, **59**, 1758.
- 32 P.E. Blöchl, *Phys. Rev. B* 1994, **50**, 17953.
- 33 H.J. Monkhorst and J.D. Pack, *Phys. Rev. B* 1976, **13**, 5188.
- 34 A. Togo, F. Oba and I. Tanaka, *Phys. Rev. B* 2008, **78**, 134106.
- 35 R. Hill, *Proc. Phys. Soc. A* 1952, **65**, 349.
- 36 N.R. Sanjay Kumar, S. Chandra, S. Amirthapandian, N.V. Chandra Shekar and P. Ch Sahu, *Mater. Res. Express* 2015, **2**, 016503.
- 37 N.R. Sanjay Kumar, N.V. Chandra Shekar, S. Chandra, J. Basu, R. Divakar and P. Ch Sahu, *J. Phys.: Condens. Matter* 2012, **24**, 362202.
- 38 J. Lu, F. Hong, W.J. Lin, W. Ren, Y.W. Li and Y.F. Yan, *J. Phys.: Condens. Matter* 2015, **27**, 175505.
- 39 L.P. Ding, P. Shao, F.H. Zhang, X.F. Huang and T.L. Yuan, *J. Phys. Chem. C* 2015, **119**, 21639.
- 40 M. Born, *Proc. Cambridge Philos. Soc.* 1940, **36**, 160.
- 41 S. F. Pugh, *Philos. Mag.* 1954, **45**, 823.
- 42 X.Q. Chen, H.Y. Niu, D.Z. Li and Y.Y. Li, *Intermetallics* 2011, **19**, 1275.
- 43 F. M. Gao, J. L. He, E. D. Wu, S. M. Liu, D. L. Yu, D. C. Li, S. Y. Zhang and Y. J. Tian,

- Phys. Rev. Lett.* 2003, **91**, 015502.
- 44 G. Kresse and D. Joubert, *Phys. Rev. B* 1999, **59**, 1758.
- 45 J.F. Nye, *Physical properties of Crystals: Their Representation by Tensors and Matrices*, Oxford University Press, New York, 1985.
- 46 P. Ravindran, L. Fast, P.A. Korzhavyi, B. Johansson, J. Wills and O. Eriksson, *J. Appl. Phys.* 1998, **84**, 4891.
- 47 R. Ahmed, F.E. Aleem, S.J. Hashemifar and H. Akbarzadeh, *Physica B* 2007, **400**, 297.

**Table 1.** Calculated elastic constants  $C_{ij}$ , bulk modulus  $B$  (GPa), EOS Fitted Bulk Modulus  $B_0$  (GPa), shear modulus  $G$  (GPa), Young's modulus  $E$  (GPa),  $B/G$ , and Poisson's ratio  $\nu$ , Debye temperature  $\Theta$  (K) for  $P6_3/mmc$ -Tc<sub>2</sub>C and  $P-6m2$ -TcC, together with other theoretical results and available experimental data.

structure		$C_{11}$	$C_{12}$	$C_{13}$	$C_{33}$	$C_{44}$	$C_{66}$	$B$	$B_0$	$G$	$E$	$B/G$	$\nu$	$\Theta$
$P6_3/mmc$ -Tc <sub>2</sub> C	this work (GGA)	612	201	172	781	199	206	343	344	216	536	1.59	0.239	675
$P6_3/mmc$ -Re <sub>2</sub> C	theor.(GGA) [11]	748	201	219	939	252	273	410	400	273	671		0.227	564
	theor. [12]							388.9						
	expt. [14]							405(30)						
	expt. [15]							386(10)						
$P-3m1$ -Ru <sub>2</sub> C	expt. [37]							178(4)						
$P-31m$ -Ru <sub>2</sub> C	theor. (GGA) [38]	500	198	239	481	151		315		139		2.27	0.307 <sup>a</sup>	
$P6_3/mmc$ -Os <sub>2</sub> C	theor. (GGA) [36]								418.48					
	theor. (GGA) [39]	639	142	329	579	111		381		152	402	2.51	0.32	
$P-6m2$ -TcC	this work (GGA)	682	200	166	940	169	241	371	372	225	562	1.65	0.247	756
	theor (LDA) [19]	749	244	211	1031	199	252	426		270		1.59	0.24	831
	theor.(LDA) [20]	752	228	199	1030	198			416	252	629		0.249	
	theor.(LDA) [21]	759	232	188	1044	188		414	416	249	623	1.67	0.249	864
$P-6m2$ -WC	expt. [5]	720	254	267	972	328		439						
$Fm-3m$ -PtC	expt. [10]							301(±15)						

<sup>a</sup> Our calculated result from Ref. [39] on the basis of  $\nu=(3B-2G)/(6B+2G)$ .

## Figure Captions

**Fig. 1** (color online) Crystal structure of the  $P6_3/mmc$ -Tc<sub>2</sub>C structure. Large and small spheres represent Tc and C atoms, respectively.

**Fig. 2** Phonon dispersion curves of the  $P6_3/mmc$ -Tc<sub>2</sub>C at 0 GPa (a) and 120 GPa (b).

**Fig. 3** (color online) Total energy versus f.u. volume for Tc<sub>2</sub>C with five different structures.

**Fig. 4** (color online) The calculated formation enthalpy-pressure curves for Tc<sub>2</sub>C with five different structures.

**Fig. 5** (color online) The calculated volume compression as a function of pressure for the  $P6_3/mmc$ -Tc<sub>2</sub>C compared with WC, PtC, Re<sub>2</sub>C, and Ru<sub>2</sub>C.

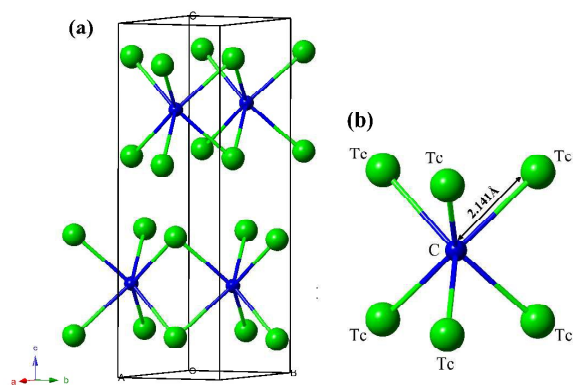
**Fig. 6** Three-dimension surface representations of the Young's modulus (a) and bulk modulus (c) in the  $P6_3/mmc$ -Tc<sub>2</sub>C. The plane projections of the directional dependence of the Young's modulus (b) and bulk modulus (d) in the  $P6_3/mmc$ -Tc<sub>2</sub>C.

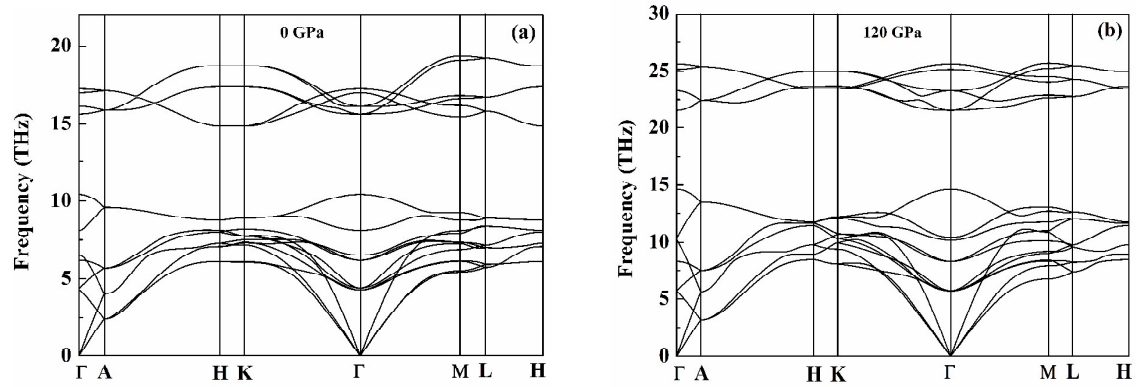
**Fig. 7** Directional dependences of Young's modulus (a) and the shear modulus (b) in the (0001), (10 $\bar{1}$ 0), ( $\bar{1}$ 012), and (1 $\bar{2}$ 12) planes.

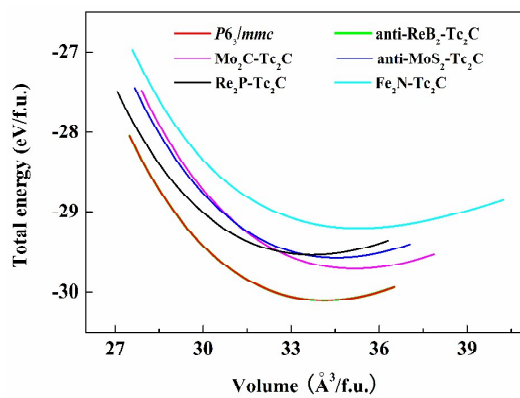
**Fig. 8** Debye temperature of the  $P6_3/mmc$ -Tc<sub>2</sub>C as a function of pressure.

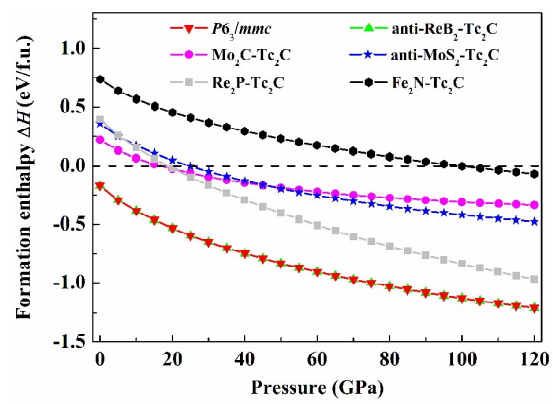
**Fig. 9** (color online) Total (a) and partial (b) densities of states of the  $P6_3/mmc$ -Tc<sub>2</sub>C. The vertical dashed line denotes the Fermi level  $E_F$ .

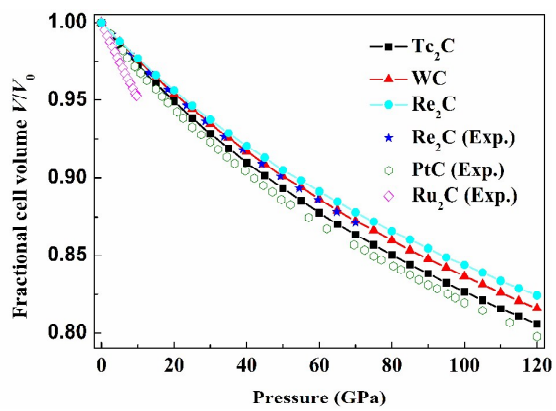
**Fig. 10** Contours of ELF of the  $P6_3/mmc$ -Tc<sub>2</sub>C on the (110) plane at 0 GPa.

**Fig. 1**

**Fig. 2**

**Fig. 3**

**Fig. 4**

**Fig. 5**

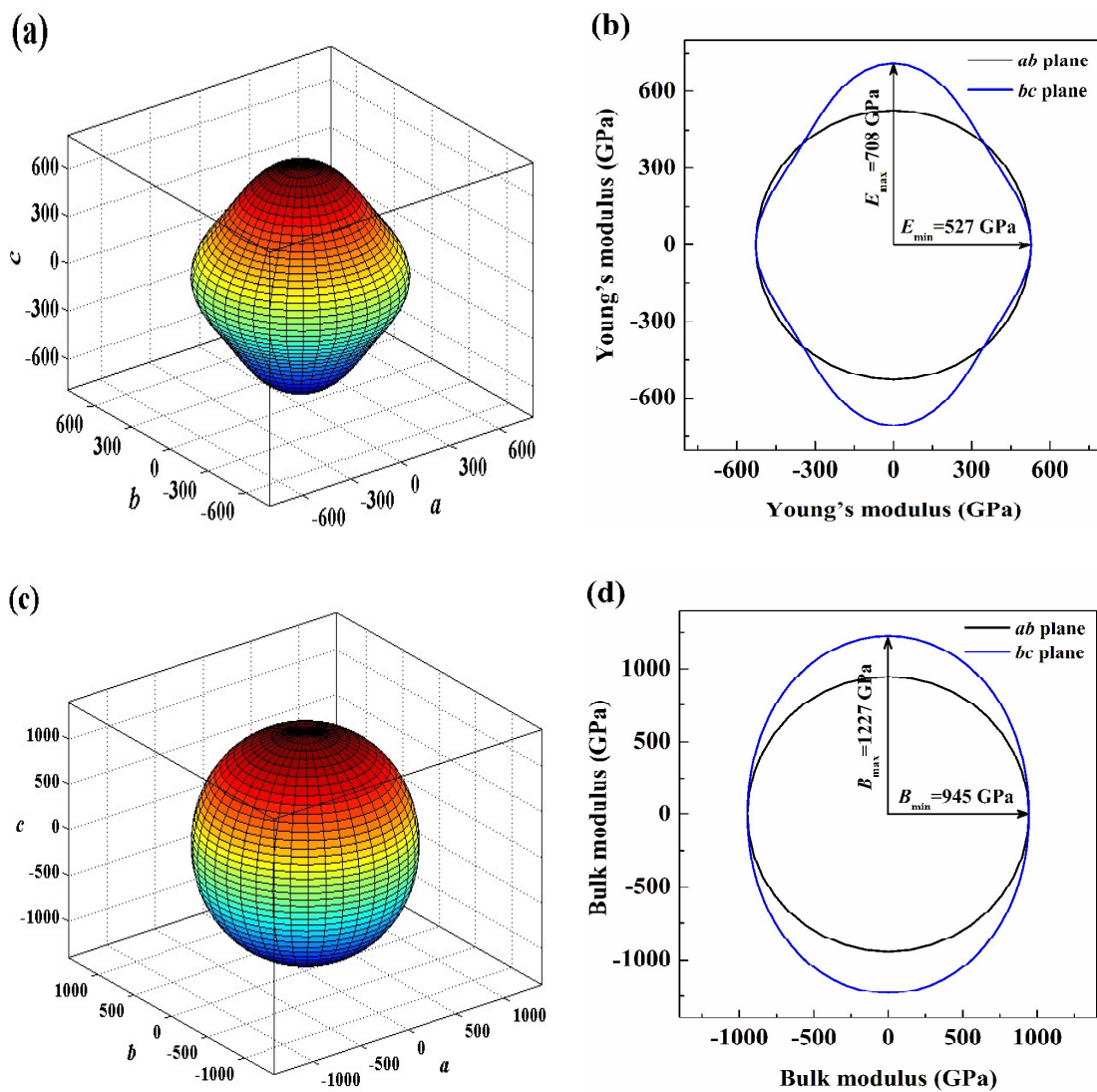


Fig. 6

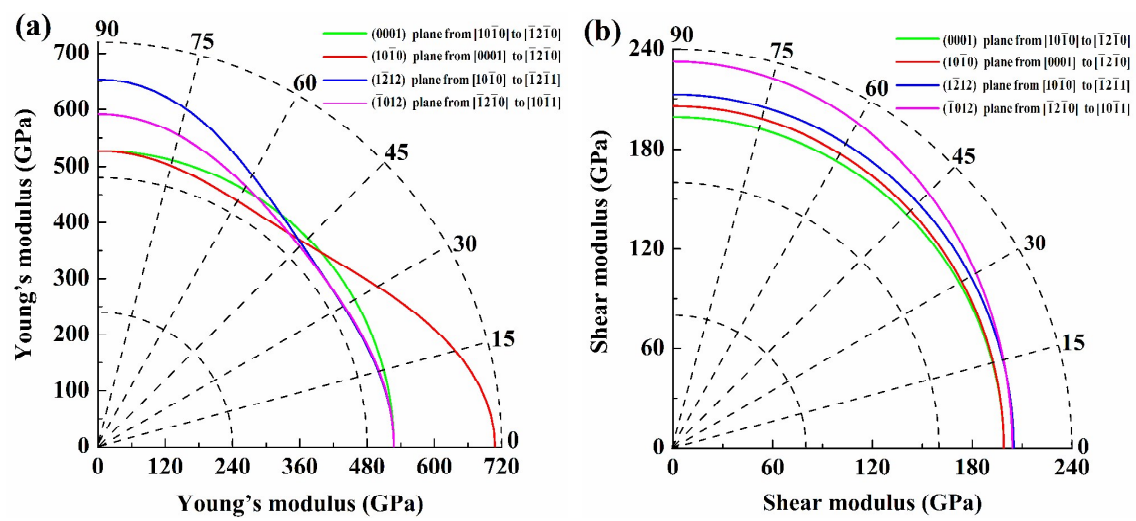
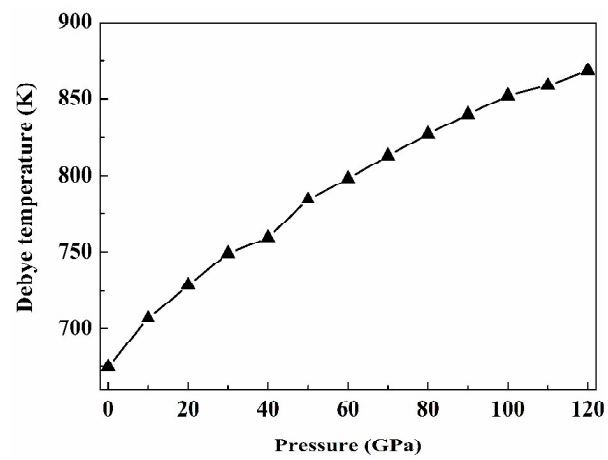
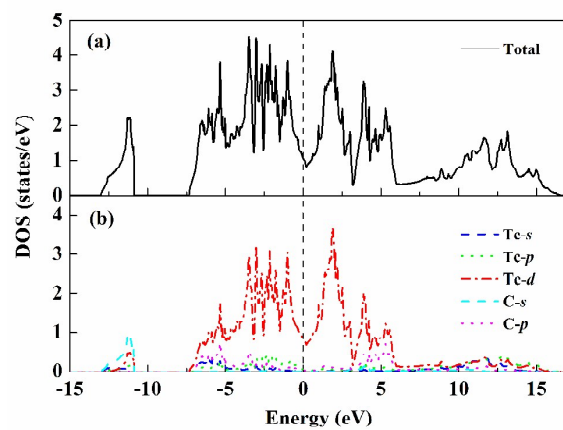
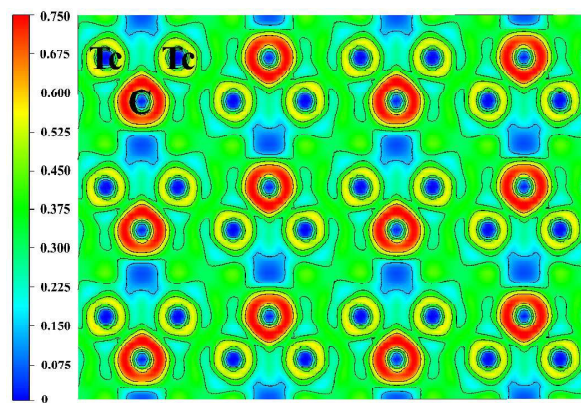


Fig. 7

**Fig. 8**

**Fig. 9**



**Fig. 10**